



Semnan University



## Research Article

# Experimental Investigation and Performance Simulation Development of a Valved Pulsejet Engine

Mohsen Sadeghi <sup>a</sup>, Elyas Lekzian <sup>a\*</sup> , Shahaboddin Kharazmi <sup>b\*</sup>,  
Mohammad Hossein Khalesi <sup>b</sup> 

<sup>a</sup> Faculty of New Sciences and Technologies, Semnan University, Semnan, 35131-19111, Iran

<sup>b</sup> Faculty of Mechanical Engineering, Semnan University, Semnan, 35131-19111, Iran

## ARTICLE INFO

### Article history:

Received: 2024-10-22

Revised: 2025-01-16

Accepted: 2025-02-15

### Keywords:

Pulse-jet engine;

Fabrication and test;

Thrust;

Specific fuel consumption.

## ABSTRACT

The objective of the present study is to conduct an empirical and theoretical investigation of a liquid-fueled laboratory hobby scale pulsejet engine. This engine comprises an inlet and air intake valve, combustion chamber, exhaust pipe, connecting semi-cone, igniter, and fuel injector. It is capable of ignition, stable combustion, and thrust production with a combustion chamber length to a total length ratio of 0.14. The operating frequency of this engine is 56 Hz, and the valves can function for 10 minutes. Experimental tests have demonstrated that the thickness of the valves significantly impacts the stable combustion of the engine. Empirical data indicate that the operating pressure ratio of the combustion chamber to ambient pressure is approximately 1.63. The average thrust of the engine is 140 Newtons, and the fuel mass flow rate is 15.9 grams per second. A performance simulation program for this engine has been developed using MATLAB software. Validation of the results shows the utmost 5/1% discrepancy between the simulation and experimental data. The simulation indicates that increasing the chamber pressure ratio from 1.5 to 2.5 results in a nearly sixfold increase in thrust. With an increase in the chamber pressure ratio, specific fuel consumption decreases. The simulation also shows that an increase in the engine's exhaust temperature leads to a reduction in thrust. Additionally, the sensitivity of thrust reduction to an increase in exhaust duct temperature is higher at elevated combustion chamber pressures. Furthermore, increasing the ratio of the combustion chamber diameter to the exhaust duct diameter results in an increase in thrust relative to the engine's baseline thrust. The specific fuel consumption of the engine increases with the combustion chamber diameter.

© 2025 The Author(s). Journal of Heat and Mass Transfer Research published by Semnan University Press.

This is an open access article under the CC-BY-NC 4.0 license. (<https://creativecommons.org/licenses/by-nc/4.0/>)

## 1. Introduction

Among all the new emerged with no-moveable parts propulsion systems, including thrusters and microthrusters [1-3], ramjet [4-6], and scramjet engines [7,8], the pulsejet engines are one of the first fabricated and the oldest ones. Pulsejet engines represent a fascinating aspect of both the history and future of propulsion technology. They offer several unique advantages

that make them appealing for various applications. One of the primary benefits of pulsejet engines is their simple construction. They can be built with few moving parts, which makes them lightweight and structurally straightforward [9]. Pulsejet engines utilize resonant combustion, meaning that the combustion process occurs cyclically and intermittently within the combustion chamber at a specific frequency. They control the expanding

\* Corresponding author.

E-mail address: [e.lekzian@semnan.ac.ir](mailto:e.lekzian@semnan.ac.ir) & [kharazmi@semnan.ac.ir](mailto:kharazmi@semnan.ac.ir)

### Cite this article as:

Sadeghi, M., Lekzian, E., Kharazmi, S. and Khalesi, M. H., 2025. Experimental Investigation and Performance Simulation Development of a Valved Pulsejet Engine. *Journal of Heat and Mass Transfer Research*, 12(2), pp. 271-286.

<https://doi.org/10.22075/JHMTR.2025.35703.1628>

combustion products through the engine's exhaust pipe in such a way that a pulsed jet stream is formed, generating thrust intermittently [10]. This unique operation allows them to function in a static manner. Overall, the pulsejet engine's main challenges are resonant combustion, combustion efficiency, valve mechanism, fuel types, and operating conditions. In this paper, the fuel types and operating conditions of a pulsejet engine are investigated.

Pulsejets can be broadly categorized into two main types: valveless [11,12] and valved [13] pulsejets. In this paper, a valve-controlled pulsejet is examined. Valve-controlled pulsejets are categorized into two types: actively controlled valves [10] and passively controlled valves [14, 15]. The valve of a pulsejet with a passive control mechanism typically opens and closes in response to changes in pressure within the chamber. From the combustion perspective, pulsejet engines can be further classified into several categories, including pulse detonation engines (PDE) [16-18], pulsejet engines (PJE), and rotating detonation engines (RDE) [19, 20]. These engines usually utilize liquid fuels, commonly employing fuels such as gasoline, Jet-A, JP-4, and ATK. The subsequent sections will review studies conducted on liquid-fuelled pulsejets.

Ghulam el al. [13] investigated a pulsejet engine with varying lengths of combustion chambers and exhaust pipes. They considered three different engine exhaust lengths, including 27, 43, and 58 centimetres. Their findings indicated that the engine performs optimally with a 43-centimeter exhaust length. Furthermore, they demonstrated that different engine designs (i.e., different engine lengths) operating at various frequencies can produce the same thrust levels. The engines they studied utilized gasoline and ethanol as fuels, revealing that gasoline provides more stable performance compared to ethanol, which poses challenges such as short-term combustion and the need for preheating due to longer combustion times. Annand et al. [15] explored the effects of different engine lengths on the performance of the combustion chamber in a pulsejet engine. They used octane as fuel for pulsejet combustion and their engines operated at a frequency range of 100-150 Hz. They investigated the behaviour of the engine using high frame-rate cameras and discovered that combustion in each operational cycle occurs due to multiple auto-ignitions that primarily happen simultaneously in different regions of the chamber. By averaging the light produced in the engine during various cycles, they created charts that illustrate the combustion and fluid dynamics (gas movement) inside the engine. They also found that pulsejet engines

function very similarly to compression ignition engines (such as diesel engines), where combustion is initiated by compressing the fuel-air mixture. In another study, Annand et al. [14] examined a butterfly valve pulsejet. They conducted laboratory experiments and analysed the flow observed using a method called SPOD, utilizing shadowgraphy. Their results indicated that two types of vortices are generated within the engine. The first is a strong, donut-shaped vortex created by the rapid closure of the engine's intake valves. The second vortex separates from the first and is generated due to the inertia of the incoming fuel and air flow. They have demonstrated that if the engine has a diverging nozzle at the end of the exhaust pipe, two distinct vortices are created at the inlet of the exhaust pipe. Additionally, they mentioned that in a straight exhaust pipe, only one vortex forms at the combustion chamber outlet. Overall, the focus of their paper was primarily on understanding the rotational flows that occur within the engine and at the beginning of the exhaust. Trzeciak and Gieras [21] calculated the exit temperature of a valveless pulsejet engine. They utilized coated thermocouples as temperature measurement sensors in the pulsejet engine, particularly at the engine outlet, due to their resistance to high gas velocities and temperature variations. They predicted a reasonable approximation of the average exit temperature of the engine by continuous measuring of the exit temperature and an iterative algorithm resulting from the obtained experimental data. They showed that even minor changes in the geometric configuration of the engine could significantly affect its behaviour, highlighting the need for precise temperature measurements in pulsejet engines. Agrawal and Pitsou [22] used ANSYS-CFX software and employed the Eddy Dissipation Model to simulate combustion within three liquid-fuel pulsejet engines. They simulated the engine with one, three, and five fuel inlets. They demonstrated that for all three models under investigation, the maximum pressure occurs in the combustion chamber, while the pressure gradually decreases within the exhaust pipe. They showed that the maximum thrust occurs in the third configuration (i.e., the engine with five fuel inlets). They came to the conclusion that the thrust generated by the pulsejet engine is dependent on the design of the fuel inlet. Anand et al. [23] examined the geometric variations affecting pressure, combustion, and frequency characteristics of a valved pulsejet engine. They considered different lengths of the exhaust pipe, the addition of a diverging nozzle at the exit, and variations in the combustion chamber length. They analyzed those effects on engine performance. They found that

except for the case where the combustion chamber is short, and the exhaust pipe is long, maximum pressure occurs in the combustion chamber, and the engine operates stably. One significant finding of their study is that when the combustion chamber is short and the exhaust pipe is long, the performance of the pulsejet engine is suboptimal, making ignition very challenging. They investigated twelve different pulsejet configurations. Some configurations exhibited stable performance, while others displayed low-frequency instability (around 25 Hz), characterized by maximum pressure fluctuations throughout the cycles. Yangster et al. [24] studied a resonant pulsed combustion chamber suitable for use in gas turbine engines. They claimed that previous research on resonant pulse combustors utilized long chambers, making their application in real gas turbine engines challenging. In their study, they focused on smaller chambers with an emphasis on pressure rise within the system. They found that both the pulse combustion section and the engine ejector could be shortened without disrupting engine performance or degrading operational parameters. Qatoumah et al. [25] investigated the performance of a pulse combustion chamber operating with liquid fuel. Their examined engine featured a combustion chamber length of 106 mm, a petal inlet diameter of 46 mm, an exhaust pipe length of 345 mm, and an exhaust pipe diameter of 38 mm. They explored the effects of fuel type on the combustion chamber, testing two fuel mixtures: one with gasoline and diesel and the other with gasoline and ethanol. They observed that the ignition delay time increased when using the gasoline-ethanol mixture compared to gasoline alone, while the ignition delay decreased when utilizing the gasoline-diesel mixture. They used the peak pressure point in the engine cycle as an indicator of heat release (or combustion) time and found that as the gasoline concentration decreased, the ignition delay for the gasoline-ethanol mixture increased almost linearly. Min et al. [26] examined the performance of a valved pulsejet utilizing liquid fuel. They investigated the effect of fuel mass flow rate on wall temperature, chamber pressure, chamber temperature, and combustion product concentration. They demonstrated that as the fuel flow rate in the engine increased, the maximum chamber pressure also rose, and the oscillation frequency of chamber performance increased. Specifically, when the fuel flow rate in this engine was increased from 7.8 liters per hour to 13.8 liters per hour, both the maximum chamber pressure and the engine frequency increased, subsequently enhancing pulse combustion. One of the key findings of their paper was that

adjusting the fuel flow rate significantly impacts the performance of the pulsejet engine and combustion characteristics. Jianpeng et al. Suganya [27] investigated the design and numerical simulation of a pulsejet that incorporates a flame holder within its chamber. The length of their pulsejet combustion chamber was 100 millimetres, the exhaust tube length was 500 millimeters, and the length of the conical section was 84.3 millimeters. Additionally, the chamber diameter was 69 millimeters, while the exhaust pipe diameter was 40 millimeters. The injection velocity of fuel into the chamber and the incoming air velocity to the engine were considered to be 82 meters per second and 72 meters per second, respectively. They demonstrated that the use of a flame holder in the engine resulted in an increase in thrust. Nazarpour and Fathali [28] investigated the impact of geometric characteristics of a valveless pulsejet engine on thrust parameters and other performance metrics. They demonstrated that for their engine if the length-to-diameter ratio of the exhaust pipe is set at 29, the length-to-diameter ratio of the combustion chamber at 25.1, and the length-to-diameter ratio of the engine inlet at 5.3, the thrust of the engine significantly increases. Taheri et al. [29] focused on the design, construction, and testing of a valveless pulsejet engine, examining the effect of geometric parameters on thrust. Their engine had an overall length of 116.74 centimeters, a combustion chamber diameter of 8.89 centimeters, and an exhaust pipe diameter of 4.5 centimeters. They reported that their engine generates a thrust of 54 Newton initially; however, they noted that the thrust value varies in subsequent cycles, with an average thrust calculated at 31 Newton. Additionally, they reported 4 bar pressure inside the combustion chamber. Rajashkar et al. [30] used shadowgraphy techniques to investigate the unsteady flow field inside the exhaust pipe as well as within the engine combustion chamber. Their pulsejet used hydrogen as fuel and operated at a frequency of 250 Hertz. Their shadowgraph observations revealed the formation of vortex rings inside the combustion chamber. They indicated a complete cycle of combustion and discharge flow from the pulsejet engine. To address the issue of non-flammability of combustion products at high pulsejet speeds, they suggested creating a barrier in the airflow path (i.e., adding a flame holder to the chamber) to provide more time for combustion. They suggested that if this pulsejet engine is used on a drone, a supplementary torch flame should be utilized at the inlet for engine start-up. They demonstrated the proper operation of their proposed design through laboratory tests and

shadowgraph observations. Evans and Alshami [31] employed a pulsejet engine in a heat-generating setup. The pulsejet engine they used was a valveless design consisting of two coaxial tubes, each measuring 76.2 cm in length with internal diameters of 3.48 cm and 4.04 cm. The combustion chamber diameter was slightly larger than that of the exhaust outlet; the combustion chamber length was 17.145 cm, while the inlet length was 15.875 cm. They stated that their designed engine possesses the capability for automatic adjustment across a wide operational range (in terms of fuel flow rate and chamber pressure). Additionally, their engine was capable of operating with liquid propane, gaseous propane, and hydrogen. Paksoon and Dagheri [32] investigated a laboratory setup referred to as a pressure gain combustor. Their setup consisted of a valve-controlled pulsejet with liquid fuel, an ejector, and a shroud tube connected to a small turbocharger, which in turn was connected to a turbine that generated thrust. The thrust produced by this system was measured using a load cell. This system was designed to investigate issues related to the interaction of pulse combustion devices with turbomachinery mechanisms. The pulsejet engine in this apparatus used liquid fuel (gasoline), operated at a frequency of approximately 220 Hz, and generated a thrust of about 4.2 pounds (18.68 Newton). The inlet valve was of the flap type, with a thickness of 0.006 inches. It was mechanical and opened and closed passively due to the pressure differential created by the combustion process and the corresponding gas dynamics occurring in the pulsejet combustion chamber and exhaust pipe. One of the weaknesses of this setup was the short operational lifespan of the pulsejet valves. Geng et al. [33] investigated a valve-controlled butterfly pulsejet. In their study, they utilized high-speed cameras to observe the operation of the valve in a 50 cm long pulsejet engine. They examined this engine using both experimental and simulation methods. Their engine, which operated on ethanol, produced an average thrust of 25 Newton at a frequency of 240 Hz. The exhaust gas velocity from the engine behaved like a wave with a frequency of 235 Hz. Their observations revealed that the valves remained open for approximately 30 percent of each cycle. The location and timing of combustion were determined by measuring CH (a molecule produced during the combustion of ethanol). Their results indicated that combustion occurred when the pressure inside the combustion chamber exceeded atmospheric pressure. Nakano et al. [34] investigated the length of the exhaust pipe on the performance of a pulsejet engine through both experimental and numerical

methods. Their findings revealed that employing a diverging nozzle (flare tube) at the exhaust pipe exit significantly increases the mass flow rate entering the engine, which in turn enhances thrust. Lightki et al. [35] tested a pulsejet engine under static conditions and compared its performance with another type of engine known as a pulsed detonation engine (PDE). Their pulsejet engine operated with a fuel flow rate ranging from 2.5 to 4.5 pounds per minute (1.13 to 2 kilograms per minute). The thrust generated by pulsejets ranged from 40 to 102 pounds (178 to 453 Newton). The maximum pressure within the combustion chamber of these pulsejets varied between 8 to 20 pounds per square inch gauge (psig) (55 to 138 kilopascals). In contrast, pulse detonation engines (PDEs) achieved significantly higher pressures of 80-120 psig (550 to 830 kilopascals). Their specific thrust was approximately 40 to 100 pounds force thrust, whereas under similar conditions, PDEs produced a specific thrust of 120 pounds force thrust. One critical aspect of experimental pulsejet testing is that the speed of sound is a function of temperature, and this parameter (i.e., temperature) varies both spatially and temporally within a pulsejet engine. Blomquist [36] accurately measured the average temperature in a pulsejet engine (a pulsed combustion chamber) using eight thermocouples. This engine was utilized for heating purposes, and his results demonstrated that it could operate and generate heat under various operational conditions. However, Blomquist pointed out that one of the significant issues with this engine is the excessive production of carbon dioxide. Mason et al. [37] investigated the combustion chamber of a valveless pulsejet engine. They analysed the flow dynamics within the chamber, including heat transfer, pressure distribution, and thermal efficiency, using both experimental and numerical methods. They categorized the flow behaviour into primary and secondary flows. The primary flow referred to the portion of the flow field describing the fluid that completes a full convective cycle from the combustion chamber's inlet to the exhaust pipe outlet. The secondary gas flow describes the fluid that does not undergo the aforementioned processes, which can be observed both at the inlet and in the exhaust pipe of the combustion chamber.

In this paper, the performance of a liquid-fueled pulsejet engine is examined. The next section explains the methodology used for laboratory testing. Then, the developed theoretical approach is reviewed. The results obtained from the theoretical method are compared and validated against experimental data from the tests conducted. Subsequently, the

effects of varying the combustion chamber diameter and pressure on engine performance, particularly thrust and fuel consumption, are investigated. Thereafter, the impact of increased temperature in the engine's exhaust section is discussed. Additionally, the influence of changes in altitude, flight speed, and fuel type on engine performance is analyzed. This engine can be used as a laboratory apparatus for studying the resonating and unsteady cyclic combustion.

The primary innovation of this paper lies in the successful construction and experimental testing of a pulsejet engine at a laboratory scale. Another innovative aspect is the development of a MATLAB simulation code that predicts the performance of pulsejet engine. This simulation tool bridges the gap between theory and practice, enabling researchers to predict engine behavior under various conditions without the need for physical testing. It combines experimental testing with simulation, establishing a reliable approach in pulsejet engine research. By integrating these two methods, this paper provides a more comprehensive understanding of pulsejet engine performance. This unified approach not only validates theoretical models but also enriches them with experimental data. Existing studies on pulsejet engines have several gaps, including: a limited understanding of long-term stability and material durability under various conditions, a lack of comprehensive analysis on how different fuel types and flow rates impact multiple performance parameters (thrust, specific fuel consumption, temperature), insufficient validation of simulation models with extensive experimental results, impacting the reliability of simulations. Spite of some studies [25,26] focused on fuel types and flow rates but did not explore the comprehensive impact on various performance parameters like thrust, specific fuel consumption, and temperature distribution, or other studies reported significant variability in thrust but did not investigate the underlying causes or ways to optimize engine design to minimize this variability. This study addresses these gaps by extending the understanding of geometric configurations by exploring the impact of valve thickness and combustion chamber pressures on both short-term and long-term stability and performance. Identifying factors contributing to thrust variability and proposing design optimizations to reduce it, including detailed analysis of the effects of combustion chamber pressure and exhaust temperature on thrust stability.

## 2. Methodology

In this section, the constructed pulsejet engine introduced, including its dimensions and

the measured parameters. Then, the theoretical approach of simulation is described.

### 2.1. Experimental Procedure

The constructed pulsejet engine consists of the following components: the inlet (Figure 1: a), intake valve, combustion chamber (Figure 1: b), a downstream conical section of the combustion chamber (Figure 1: b), the exhaust duct of the engine (Figure 1: b), and fuel injection nozzle (Figure 1: c), spark plug (Figure 1: d). The overall configuration of the engine is depicted in Figure 1: e. The diameter of the combustion chamber is 168 mm, while the diameter of the exhaust duct is 128 mm. The ignition system of the engine includes a 230-volt transformer and a single-electrode spark plug with an electrode-base gap of 0.2 mm. The fuel system comprises a fuel pump connected to a fuel injector with a spray angle of 90 degrees. For the experimental testing of the engine, a thrust (single-component) stand was utilized to measure the thrust generated by the engine. Furthermore, the starting air pressure, and fuel pressure were measured during the experimental tests. The starting air pressure sensor was used for engine ignition and was not included in the analytical calculations. The load cell sensors measuring thrust and the fuel pressure sensor were employed for theoretical calculations in this study. The displayed values were initially compared with those from two other calibrated sensors at an atmospheric pressure of 0.85 bar under laboratory conditions to calibrate the sensors. Additionally, prior to commencing the experiments, the values indicated on the displays were considered offset values and were subtracted from the values obtained during testing.

### 2.2. Theory

According to Figure 2, the pulsejet engine consists of four wave series: a compression wave traveling to the left (toward the combustion chamber), an expansion wave moving to the right (toward the engine's exhaust), an expansion wave moving to the left, and a compression wave moving to the right. These waves oscillate within the duct at a speed slightly exceeding the local speed of sound during each operational cycle. For a pulsejet engine, the following regions can be identified: Region 4, which has maximum pressure  $P_4$  and maximum temperature  $T_4$  and is located before the expansion wave R. Region 3b, which is positioned after the expansion wave, experiences a decrease in both pressure and temperature. Region 3a due to changes in the engine cross-sectional area, exhibits different characteristics compared to Region 3b. Region 1, known as the base region, is located in the

engine's exhaust pipe, where its pressure  $P_1$  is close to atmospheric pressure, and its initial temperature  $T_1$  equals the ambient temperature; however, this temperature increases with engine operation. Additionally, a contact surface exists between the compression wave and the expansion wave [38-40]. The contact surface is located between the discontinuity of Regions 2 and 3a.

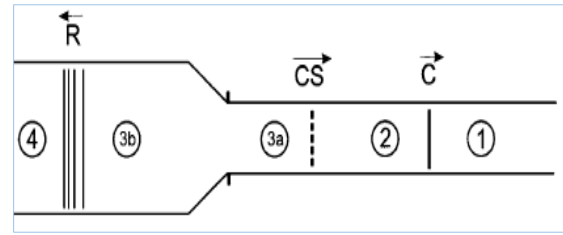


Fig. 1. Schematic of wave areas in engine

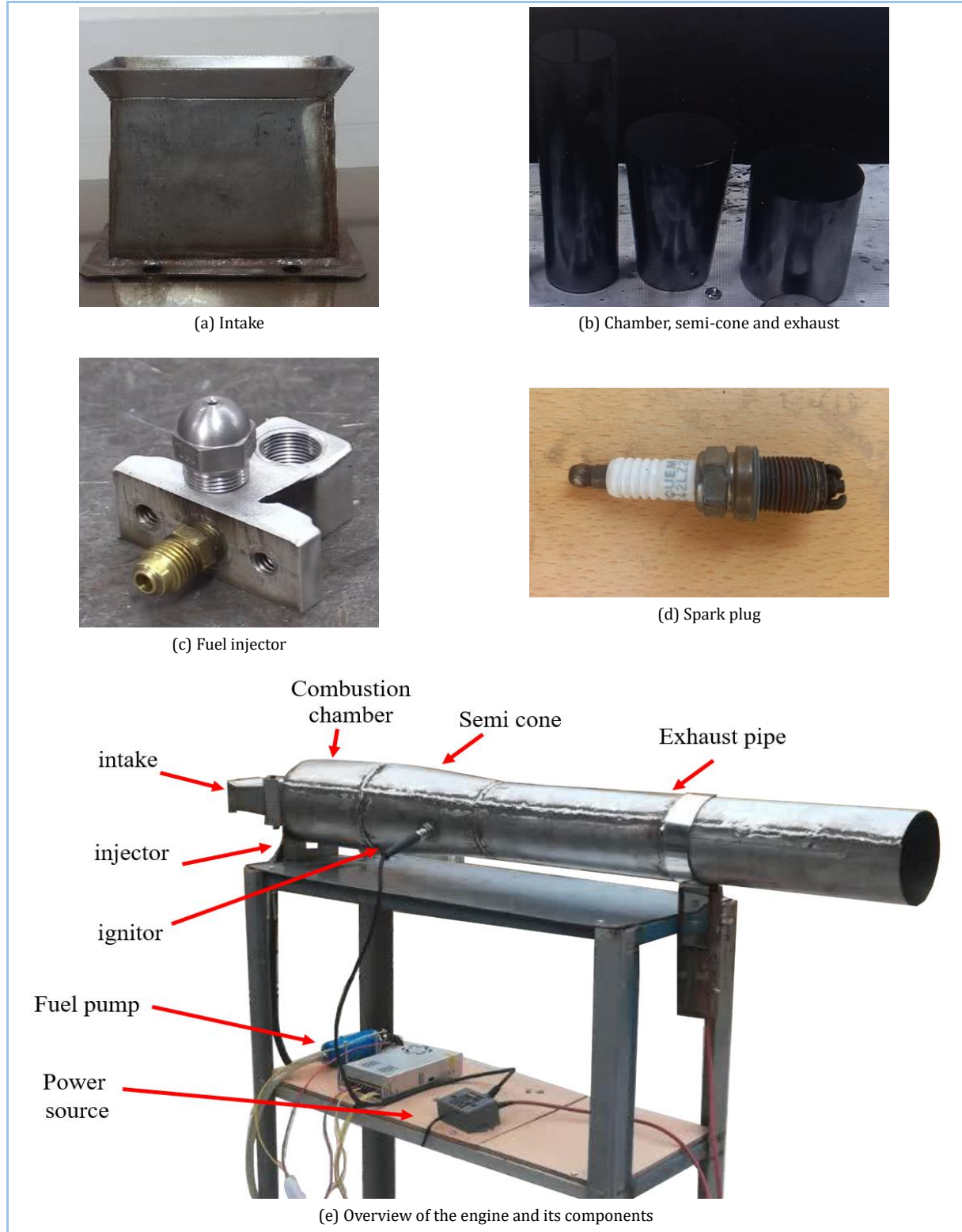


Fig. 2. Pulsejet engine main components (test stand not shown)

In this paper, only the main equations for engine analysis are presented. The period of each cycle is calculated using equation (1). The duct length ( $l_{c/p}$ ) refers to the combined length of the combustion chamber and the engine's exhaust duct.

$$\Delta t_{cyc} = \frac{4l_{c/p}}{a_1} = \frac{1}{f_{cyc}} \quad (1)$$

where  $f_{cyc}$  is the operational frequency, and  $a_1$  denotes the speed of sound in region 1. It is assumed that thrust and pressure inside the combustion chamber oscillate around a mean value. Consequently, a maximum thrust is denoted by  $F_{max}$ , and an average thrust is represented as  $\bar{F}$ . The average thrust is related to the maximum thrust as the following:

$$\bar{F} \approx \frac{F_{max}}{\pi} \quad (2)$$

The mass flow rate of fuel consumed by the engine is in the following:

$$\dot{m}_f = \left(1 - \frac{T_4}{T_1}\right) \left[ \frac{\rho_c \nabla_c C_p T_1}{\Delta t_{c,i} h_{PR} \eta_b} \right] \quad (3)$$

where  $\rho_c$  represents the density in the combustion chamber,  $\nabla_c$  denotes the volume of the combustion chamber,  $h_{pr}$  is the heating value of the fuel,  $\eta_b$  signifies the combustion chamber efficiency, and  $\Delta t_{c,i}$  indicates the time required for combustion within the chamber. The ratio of the cross-sectional area of the combustion chamber to that of the exhaust duct can also be calculated using the energy balance between these two regions along with gas dynamics relations as follows:

$$\frac{A_{cc}}{A_d} = \frac{Ma_{3a}}{Ma_{3b}} \left[ \frac{2 + (\gamma - 1) Ma_{3b}^2}{2 + (\gamma - 1) Ma_{3a}^2} \right]^{\frac{\gamma + 1}{2(\gamma - 1)}} \quad (4)$$

where  $Ma_{3a}$  and  $Ma_{3b}$  are the Mach numbers in regions 3a and 3b. There exists a contact region (or surface) between Region 2 (i.e., after the compression wave moves towards the engine outlet) and Region 3a. This contact surface moves at a local speed of sound towards the engine outlet, and the following assumptions are considered for this region:

$$u_{3a} = u_2, \quad P_{3a} = P_2 \quad (5)$$

$$a_{3a} \neq a_2, \quad \rho_{3a} \neq \rho_2 \quad (6)$$

Using the relations pertaining to the expansion wave between regions 3b and 4, as well as the equations of state for an ideal gas and isentropic processes, an equation for the speed of sound in region 3a can be calculated as follows:

$$a_{3a}^A = a_1 / \left[ \frac{a_1}{a_4} \left( \frac{P_4}{P_1} \right)^{\frac{\gamma - 1}{2\gamma}} - \frac{\gamma - 1}{2} Ma_{3a} \right] \quad (7)$$

Additionally, by employing the energy conservation between the area change regions of the engine (regions 3a and 3b), an equation for the speed of sound at region 3a is derived as follows:

$$a_{3a}^B = a_{3b} \left( \frac{1 + \frac{\gamma - 1}{2} Ma_{3b}^2}{1 + \frac{\gamma - 1}{2} Ma_{3a}^2} \right)^{\frac{1}{2}} \quad (8)$$

The values of other parameters such as pressure or temperature are computed using isentropic relations and the ideal gas equation. The thrust generation phase corresponds to a scenario where an expansion wave is propagating toward the combustion chamber (see Figure 3).

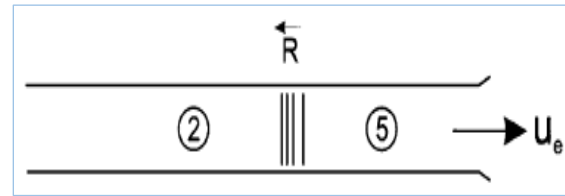


Fig. 3. Schematic of engine thrust production positions in the phase of the expansion wave in the outlet tube

The following equation is derived between the upstream and downstream of the expansion wave:

$$u_5 \approx u_2 + \frac{2(a_2 - a_1)}{\gamma - 1} \quad (9)$$

Therefore, the maximum thrust can be computed as follows:

$$F_{max} = \dot{m}_e (u_e - V_\infty) = \rho_5 u_5 A_p (u_5 - V_\infty) \quad (10)$$

The algorithm for the overall performance analysis of the engine is illustrated in figure 4.



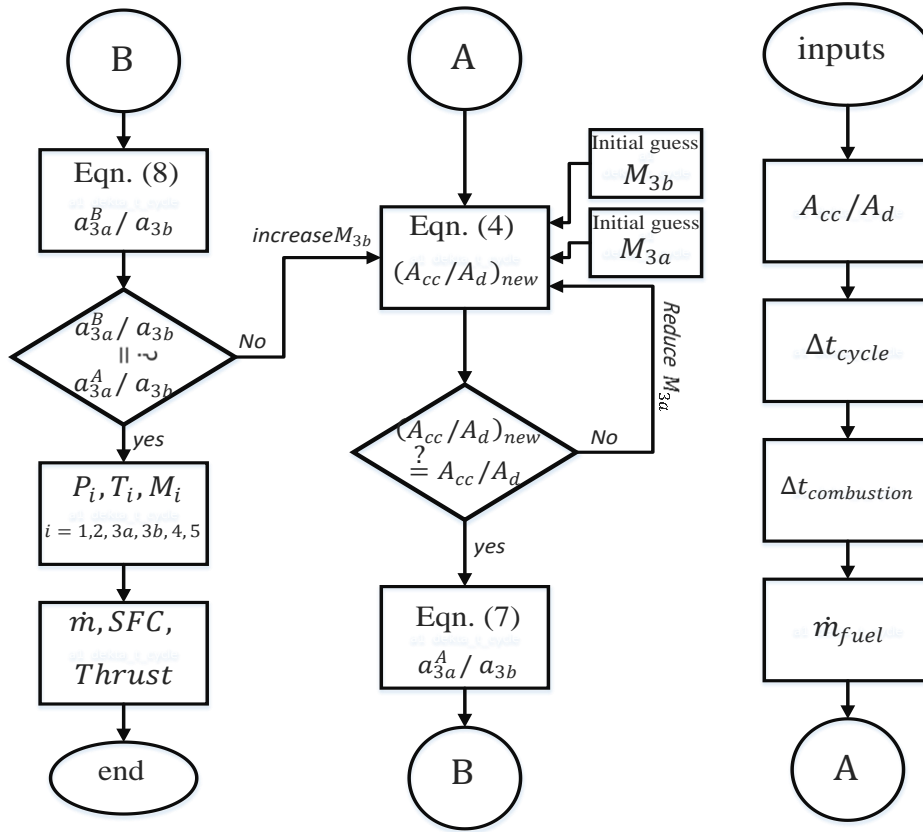


Fig. 4. Engine performance analysis algorithm

2.3. Theory Assumptions

1. It is assumed that the velocity in region 4,  $u_4$ , is zero.
2. There is a contact wave that moves to the right (a wave between the incident and reflected waves of expansion and compression). It is assumed that in the direction of this wave  $u_{3a} = u_2$  and  $p_{3a} = p_2$ , but it should be noted that  $\rho_{3a} \neq \rho_2$  and  $a_{3a} \neq a_2$ .
3. It is assumed that the velocity in region 1,  $u_1$  is zero.
4. It is assumed that at the engine exit  $p_1 = p_5 = p_{amb}$ .
5. The following assumptions are considered between regions 1 and 5:  $a_1 = a_5$ ,  $T_1 = T_5$ ,  $\rho_1 = \rho_5$ . It is worth mentioning that at the beginning of the engine start-up,  $T_1 = T_5$ , and as the engine operates, the value of  $T_5$  increases.

3. Validation

To comprehensively assess the performance of this engine, simulation outputs are validated against experimental results. The inputs for the simulation program are listed in Table 1.

Table 1. Pulsejet performance simulation input parameters

Parameter	Description	unit	value
$d_{cc}$	CC Dia.	m	0.168
$d_{tail}$	Exhaust Dia.	m	0.128
$l_{cc}$	CC length	m	0.2
$l_t$	total Length	m	1.46
$T_1$	Ambient temp.	K	300
$\rho_1$	Ambient Density	$kg/m^3$	0.988
$\eta_b$	CC efficiency	Dimless.	0.98
$p_{amb}$	Ambient press.	Pa	85000
$\gamma$	Specific heat ratio	Dimless.	1.33
$h_{PR}$	Heating value	MJ/kg	40

Moreover, the outputs of this simulation include those specified in Table 2. The subscripts  $i=1, 2, 3a, 3b, 4, 5$  refer to different locations within the pulsejet engine, as explained in Section 2-2.

Table 2. Simulation outputs

Parameter	Description	unit
$M_i$	Mach at station i	Dimless.
$P_i$	Press. At station i	kPa
$T_i$	Temp. at station i	K
$F_{peak}$	Maximum thrust	N
$F_{avg}$	Average thrust	N
$\dot{m}_f$	Fuel flow	g/s
$\dot{m}$	Mass flow rate	kg/s
TSFC	Specific fuel consumption	kg/hr-N



In Table 3, the simulation results are compared with laboratory values, and the following conditions demonstrate that the results exhibit a maximum discrepancy of 5.1% from laboratory values. It should be noted that the error is calculated from the following equations:

$$e_{thrust} = |F_{avg,exp} - F_{avg,theory}| / F_{avg,exp} \quad (11)$$

$$e_{\dot{m}_{fuel}} = |\dot{m}_{avg,exp} - \dot{m}_{avg,theory}| / \dot{m}_{avg,exp} \quad (12)$$

The maximum error for the thrust value based on experimental data is 1.75%, while for the fuel mass flow rate, it is 1.5%. The average difference between the simulated and the laboratory thrust average is 0.6%. The average difference between the simulated mass flow rate of the fuel and the average mass flow rate obtained from experiments is 0.2%. This level of discrepancy for all these parameters appears acceptable according to the analytical methodology developed in this paper, and results from other simulations of this engine, which will be discussed in the next section, can be used to examine the behavior of the constructed engine with a maximum error percentage of 1.75%.

**Table 3.** Comparison of simulation and laboratory test results

Experiment Results			Simulation Results			errors	
Thrust (N)	$\dot{m}_{fuel}$ (g/s)	$p_4/p_1$	Thrust (N)	$\dot{m}_{fuel}$ (g/s)	$cc_{ign}$	$e_{thrust}$	$e_{\dot{m}_{fuel}}$
135	12.86	1.62	134.5	12.2	7	-0.37	-5.1
143	14.591	1.64	142.03	14.4	8	-0.68	-1.31
168.25	16.891	1.71	169.35	16.9	8.5	0.65	0.05
142.8	17.109	1.64	142.03	17.1	9.5	-0.54	-0.05
104	13.263	1.53	102.2	13.4	9	-1.73	1.03
136.89	16.096	1.62	134.5	15.7	9	-1.75	-2.46
141.33	16.94	1.64	142.03	17.1	9.5	0.50	0.94
143.09	16.927	1.64	142.03	17.1	9.5	-0.74	1.02
143.5	16.921	1.64	142.03	17.1	9.5	-1.02	1.06

#### 4. Results and Discussion

The important input values for the engine performance simulation program are presented in Table 1. Additionally, the value of  $\frac{p_4}{p_1}$  is selected equal to 1.63. The parameter of  $cc_{ign}$  (which determines the fraction of time relative to a complete cycle duration required for the reaction to occur) is 9. The outputs of the engine performance simulation are detailed in Table 4.

In Region 1, according to initial assumptions, the Mach number is ignorable, with pressure and temperature also at ambient levels. Therefore, the baseline engine conditions correspond to the environmental conditions at the beginning of the combustion process, where the engine's exhaust duct has yet to reach a temperature higher than that of the environment; hence, the value of  $F_{peak}$  is reported as well.

Region 2 follows the compression wave exiting from the engine - (toward the engine exhaust). As expected, its pressure increases to 139.34 kPa, with a temperature rise of 11.81 Kelvin. Due to the presence of a contact surface between the compression wave and the

expansion wave regions, there exists a singularity area in this section where, according to assumptions, pressure and velocity are equal in these two regions, but density differs.

The Mach number in Region 3a is higher than in Region 3b, as expected, due to the decrease in the cross-sectional area of the engine. The pressure in Region 3a is slightly lower than in Region 3b, while temperatures are approximately equal.

The pressure in Region 4 reaches its maximum, which corresponds to that part of the combustion chamber that achieves peak pressure after valve closure. Due to the pressure increase, the temperature rises as well due to its direct relationship with pressure, reaching 469.75 Kelvin. Furthermore, according to assumptions, velocity in this region is considered negligible. The maximum thrust of this engine is calculated to be 433.61 Newtons, while its average thrust is calculated at 138.09 Newtons.

The mass flow rate of fuel for this engine is determined to be 15.9 grams per second, and the mass flow rate of incoming air is calculated at 2.68 kilograms per second.

The specific fuel consumption of this engine is 0.00011 kilograms per hour-Newtons.

**Table 4.** Simulation outputs

Parameter	unit	value
$M_4$	Dimless.	$\approx 0$
$P_4$	kPa	165.34
$T_4$	K	469.75
$M_5$	Dimless.	0.49
$P_5$	kPa	85000
$T_5$	K	300
$F_{peak}$	N	433.61
$F_{avg}$	N	138.09
$\dot{m}_f$	g/s	15.9
$\dot{m}$	kg/s	2.68
TSFC	Kg/hr-N	0.00011
$M_1$	Dimless.	0
$P_1$	kPa	85
$T_1$	K	300
$M_2$	Dimless.	0.234
$P_2$	kPa	139.34
$T_2$	K	311.81
$M_{3a}$	Dimless.	0.195
$P_{3a}$	kPa	139.34
$T_{3a}$	K	450.22
$M_{3b}$	Dimless.	0.111
$P_{3b}$	kPa	142.87
$T_{3b}$	K	453.03

#### 4.1. Combustion Chamber Pressure Ratio

The analysis of the effect of the combustion chamber pressure ratio relative to the baseline conditions of the engine is conducted in this section. Based on Figure 5, it is clear that as the chamber pressure increases, thrust also increases. An increase in chamber pressure essentially translates to an increase in flow energy, and a higher energy flow will produce greater thrust. Importantly, the engine thrust is very sensitive to changes in the pressure ratio. As the pressure ratio increases; specifically, increasing the pressure ratio from 1.5 to 2.5 results in an almost sixfold increase in thrust. Changes in the chamber pressure ratio also significantly affect specific fuel consumption, with an increase in the pressure ratio leading to a decrease in fuel consumption.

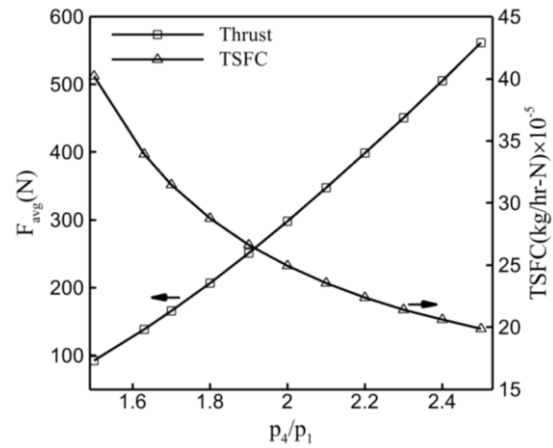


**Fig. 5.** Variations of thrust and specific fuel consumption with chamber pressure ratio

This issue arises because part of the engine thrust is provided by the energy of high-pressure air and not solely by burning fuel. Theoretically, one must also consider the formula for calculating specific fuel consumption (SFC), given by the following relation:

$$TSFC = \frac{\dot{m}_f}{F} \tag{13}$$

It can be observed that specific fuel consumption has an inverse correlation with thrust.

Additionally, according to the graph in Figure 6, changes in fuel mass flow rate with the combustion chamber pressure ratio show that as the combustion chamber pressure increases, the fuel mass flow rate also increases. The simultaneous effect of increased fuel consumption and increased thrust results in changes in specific fuel consumption.

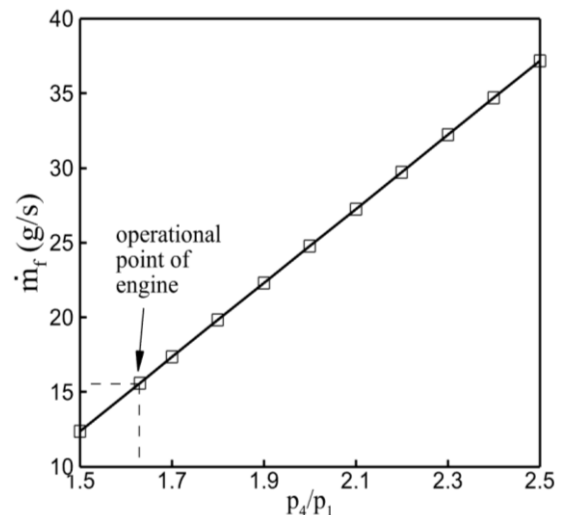


**Fig. 6.** Fuel mass flow rate changes with increasing chamber pressure

#### 4.2. Chamber to Exhaust Diameter Ratio Effect ( $d_{cc}/d_{tail}$ )

The thrust value for the baseline condition is 138.1 Newtons. In this condition, the combustion chamber diameter is 128 millimeters, and the exhaust duct diameter is 108 millimeters. The diameter of the chamber varies from 108 millimeters to 270 millimeters. As the ratio of the combustion chamber diameter to the exhaust duct diameter increases, the thrust relative to the baseline thrust of the engine increases. Additionally, fuel consumption also increases (Figure 7).

The increase in thrust is because a larger combustion chamber allows for a greater mixture of air and fuel to combust. This results in a higher volume of exhaust gases being expelled, which increases the thrust produced by the engine.

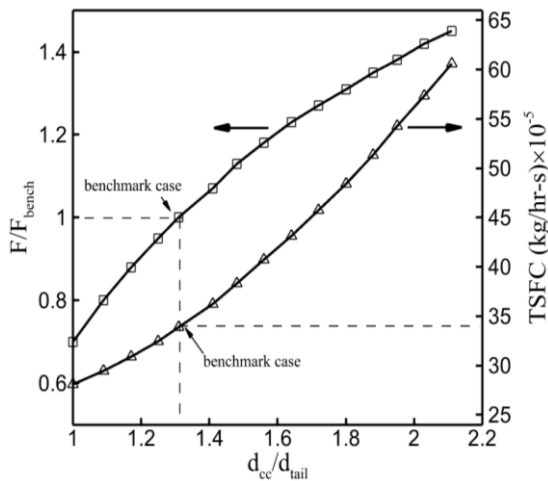


Fig. 7. Changes in thrust and specific fuel consumption with changing the ratio of chamber diameter to exhaust pipe diameter

The graphs in Figure 8 confirm that as the combustion chamber diameter increases, both fuel and air flow rates also increase. In Figure 8, the values of  $\dot{m}_{f,bench} = 15.9 \text{ g/s}$  and  $\dot{m}_{air,bench} = 2.68 \text{ kg/s}$  and mass flow rates for air and fuel are normalized. The graph illustrating changes in specific fuel consumption with varying chamber diameters (Figure 7) indicates that as the chamber diameter increases, specific fuel consumption also rises. This implies that the engine consumes more fuel to maintain a larger combustion process (in terms of volume and flow rates of fuel and air).

Therefore, although this increase in combustion chamber diameter leads to increased thrust, it also results in higher fuel consumption per unit of thrust, indicating an increase in specific fuel consumption (SFC).

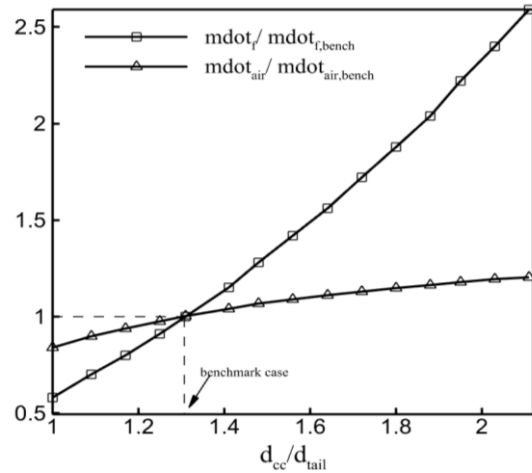


Fig. 8. Changes in mass flow rate of fuel and air with the change of combustion chamber

#### 4.3. Engine Warm Thrust

The term 'engine warm thrust' refers to the condition where the temperature in the  $T_5$  region increases. In this section, we will show that an increase in  $T_5$  temperature leads to a reduction in thrust. To analyze the engine warm thrust, certain modifications are made in the equations. It is assumed that  $u_5$  at the downstream of the expansion wave is approximately equal to the exit velocity and can be approximated by  $u_e$ . It can also be assumed that  $p_5$  and  $p_e$  are close to atmospheric pressure and are equal to  $p_1$  in this condition. The assumption is that the velocity in the exhaust duct has not reached the speed of sound, and the flow in the exhaust is not choked. Using the theory of characteristics, we can write.

$$u_2 + \frac{2a_2}{\gamma - 1} = u_5 + \frac{2a_5}{\gamma - 1} \tag{14}$$

Considering the temperature for exit from the engine duct, denoted as  $T_5$ , and based on the equation of sound speed and temperature, simply one can write the following equation:

$$a_5 = \sqrt{\gamma RT_5} \tag{15}$$

Thus, the exit velocity is written as follows:

$$u_5 = u_2 + \frac{2(a_2 - \sqrt{\gamma RT_5})}{\gamma - 1} \tag{16}$$

Subsequently, the maximum thrust can be calculated according to Equation (10). It should be noted that the value  $\rho_5$  in Equation (10) is derived from the ideal gas relationship. The variations in engine thrust with changes in exhaust temperature are illustrated in Figure 9. It is evident that as combustion chamber pressure increases at a  $T_5$  constant temperature, thrust also increases.

Figure 9 contains two important observations. The first point is that engine thrust is highly sensitive to exhaust temperature. It is observed that at a constant chamber pressure, an increase in  $T_5$  significantly reduces thrust. Therefore, thrust sensitivity to  $T_5$  changes is substantial. This highlights the importance of cooling requirements for the engine's exhaust duct. In experimental tests of this engine, when the exhaust duct was cooled with water, higher thrust values were achieved.

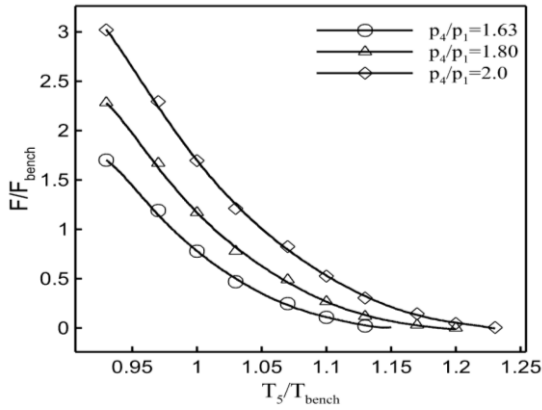


Fig. 9. Thrust variation with engine exhaust temperature

The second point from Figure 9 is that as chamber pressure ( $p_4/p_1$ ) increases, the maximum temperature ( $T_5$  maximum value) at which the engine can produce thrust also rises. If the engine shuts down during flight for any reason (such as a failure of the intake valve), the exhaust duct may have a temperature higher than ambient conditions. Consequently, it is possible for the engine to shut down after heating up air in region 5 (i.e., an increase in  $T_5$ ) and require a restart. Under such conditions, higher chamber pressure is needed to restart the engine. For example, in Figure 9, if  $T_5/T_{bench} = 1.17$  and a thrust equivalent to produce a thrust equivalent to  $\frac{F}{F_{bench}} = 0.13$  is required, then  $p_4/p_1$  must be at least 2.0. Another solution could involve reducing the temperature of air in region 5 (i.e.,  $T_5$ ), which somewhat occurs due to the cold air entering during engine shutdown; however, for a reliable restart under such conditions, it is preferable to increase the chamber pressure.

#### 4.4. Altitude and Speed Variation Effects

Considering a standard atmosphere for the pulsejet engine, the effects of altitude are analyzed. Altitude impacts pressure, density, and ambient temperature as following [41]:

$$T_{amb}(K) = (15.04 - 0.00649 h) + 273.15 \quad (17)$$

$$P_{amb}(kPa) = 101.325 \times \left[ \frac{T_{amb}(K)}{288.08} \right]^{5.256} \quad (18)$$

Results indicate that with an increase in flight speed, the thrust of the engine decreases (Figure 10-a). The reason for this is that as flight speed increases, the term  $V_\infty$  in the  $F_{ideal,max} = \dot{m}_e(u_e - V_\infty)$  diminishes, leading to a reduction in thrust. It should be noted that the behavior of thrust reduction is linear and resembles that of turbofan engines, where thrust decreases with increasing speed [42-45]. Furthermore, it is observed that at a specific speed, thrust decreases with increasing altitude. This is because as altitude increases, the density of the air entering the engine decreases, resulting in a reduced mass flow rate into the engine. For sea level altitudes 800 meters, 1600 meters, and 2000 meters, the mass flow rates into the engine are approximately 2.68 kg/s, 2.46 kg/s, 2.26 kg/s, and 2.16 kg/s, respectively. According to the law of conservation of mass, the mass flow rate exiting the engine ( $\dot{m}_e$ ) also decreases with a decrease in height. Thus, the term  $\dot{m}_e$  in the thrust equation decreases and consequently leads to a reduction in thrust.

As illustrated in Figure 10-b, fuel consumption increases with an increase in flight speed (due to the inverse correlation between thrust and specific fuel consumption). Another important point is that the sensitivity of thrust to speed elevation is higher than the sensitivity of specific fuel consumption to flying speed.

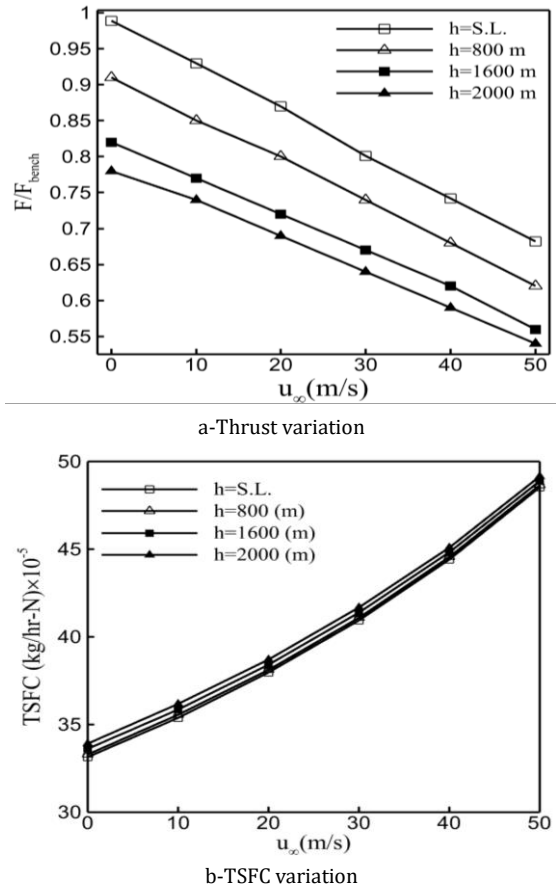


Fig. 10. Thrust and SFC variation with flying velocity

#### 4.5. Fuel Type Variation

Although it is evident that an increase in fuel calorific value leads to a reduction in fuel consumption, several different fuels with varying calorific values are examined to quantitatively assess this issue and their effects on engine performance. It is essential to mention that the use of certain fuels, such as hydrogen, presents challenges such as storage, high flammability, and toxicity issues, which are not addressed in these analyses, and only their calorific value effects are considered. Figure 11 shows that for bioethanol, kerosene, gasoline, diesel, and hydrogen fuels, the respective fuel consumption rates are 21.2 g/s, 14.8 g/s, 14.5 g/s, 14.1 g/s, and 5 g/s. It is evident that hydrogen exhibits the lowest fuel consumption in producing an equivalent amount of thrust among these five proposed fuel types. The maximum fuel consumption corresponds to bioethanol. When hydrogen is used as fuel, approximately 76% less fuel is consumed compared to using bioethanol. This highlights the importance of utilizing high-calorific value fuels. However, it should be noted that the use of hydrogen is still not common in air-breathing engines and poses numerous challenges regarding unintended flammability and storage.

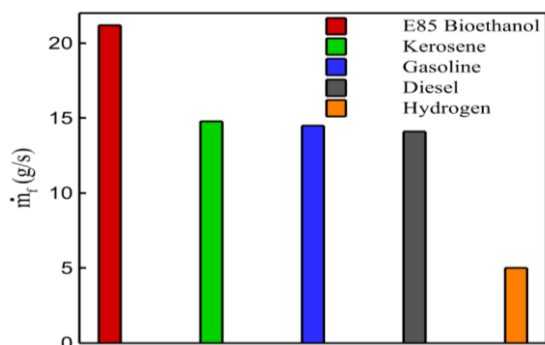


Fig. 11. Fuel flow rate variation for different fuel types

## 5. Conclusions

This study focused on the construction and performance evaluation of a pulsejet engine. The following results were obtained from the experimental tests:

1. **Combustion Chamber Pressure:** The pressure within the combustion chamber has a significant impact on the engine's performance. As the pressure increases, the engine's operational capability improves. However, structural considerations must also be taken into account, as the engine generates high temperatures upon ignition, leading to elevated chamber temperatures. Thus, pressure control is essential to prevent engine explosions.

2. **Thrust and Fuel Consumption:** Experimental results indicated that this engine produces a thrust of approximately 140 Newtons, with a fuel mass flow rate of about 15.9 grams per second.
3. **Fuel-to-Air Ratio:** In addition to the length ratio, the fuel-to-air ratio is another important parameter for ignition and stable engine performance. This engine ignites at a fuel flow rate of 15.9 grams per second and maintains a stable cycle.

The theoretical simulation results of the engine also yielded the following findings:

- 1) Increasing the pressure ratio of the engine combustion chamber to the ambient pressure results in an increase in thrust. For a condition where the pressure ratio of the chamber to the ambient is 2.5, the thrust is 6.2 times that of the condition where the pressure ratio is 1.5. Additionally, the specific fuel consumption (SFC) for the condition where the pressure ratio is 2.5 is 0.3 times that of the condition where the pressure ratio is 1.5.
- 2) The fuel consumption for the condition where the pressure ratio of the chamber to the ambient is 2.5 is 3 times that of the condition where the pressure ratio is 1.5. From points 1 and 2, it can be concluded that increasing the chamber pressure increases both thrust and fuel flow rate but reduces SFC (specific fuel consumption)
- 3) **Pressure Ratio Impact:** Similar to experimental results, increasing the combustion chamber pressure leads to an increase in thrust. For a pressure ratio of 2.5, the thrust is approximately six times greater than that at a pressure ratio of 1.5.
- 4) **Combustion Chamber Diameter:** If the diameter of the combustion chamber is doubled, thrust increases by 1.45 times, while specific fuel consumption increases by 1.8 times compared to the baseline condition. Additionally, the air and fuel mass flow rates increase by 1.2 and 2.6 times, respectively, relative to the baseline condition.
- 5) **Exhaust Air Temperature:** An increase in the temperature of the exhaust air duct leads to a reduction in thrust. For instance, when the pressure ratio is 2, increasing the exhaust temperature from 280 K to 328 K results in the thrust decreasing significantly, from three times the baseline to 0.13 times the baseline.

- 6) High-Temperature Operation: Increasing combustion chamber pressure allows the engine to operate at higher exhaust temperatures while still producing thrust.
- 7) Altitude Effects: An increase in altitude results in reduced thrust and increased specific fuel consumption. In other words, the engine performs better at lower altitudes.
- 8) Higher Heating Value Fuels: Utilizing fuels with higher heating values results in reduced fuel consumption for a given amount of thrust produced. Thus, as the heating value of the fuel increases, specific fuel consumption (SFC) decreases.

In future research on this engine, the fuel system can be configured so that injection only occurs when the valves are closed. Additionally, this system can be enhanced with exhaust duct cooling to improve performance.

## Nomenclature

$l_{c/p}$	Duct length (m)
$f_{cyc}$	Operational frequency (Hz)
$F_{max}$	Maximum thrust (N)
$\dot{m}_f$	Mass flow rate of fuel consumed(kg/s)
$\rho_c$	Combustion chamber density( $kg/m^3$ )
$V_c$	Volume of the combustion chamber( $cm^3$ )
$h_{pr}$	Heating value of the fuel (MJ/kg)
$\eta_b$	Combustion chamber efficiency
$\Delta t_{c,i}$	Time required for combustion in the chamber (s)
$M_{3a}$	Mach number in region 3a
$M_{3b}$	Mach number in region 3b

## Funding Statement

This research did not receive any specific grant from funding agencies in the public, commercial, or not-for-profit sectors.

## Conflicts of Interest

The author declares that there is no conflict of interest regarding the publication of this article.

## Authors Contribution Statement

*Mohsen Sadeghi*: Writing – review & editing.

*Elyas Lekzian*: Supervision, Writing – review & editing; Writing – original draft; Visualization; Resources; Investigation; Data curation; Conceptualization; Software.

*Shahaboddin Kharazmi*: Writing – review & editing.

*Mohammad Hossein Khaledi*: Writing – review & editing.

## References

- [1] Parhizkar, H., Ebrahimi, A., and Lekzian, E., 2017. Applying a DSMC solver to explore the effects of heater plates/wall heating in microthruster. *Modares Mechanical Engineering*, 16(11), p. 123-134. <http://dorl.net/dor/20.1001.1.10275940.1.395.16.11.21.4>
- [2] Lekzian, E., Parhizkar, H and Ebrahimi, A., 2018. Study of the effects of preheated wall/plates in microthruster systems. *Journal of Theoretical and Applied Mechanics*, 56(3), p. 713-725. <https://doi.org/10.15632/jtam-pl.56.3.713>
- [3] Lekzian, E., Ebrahimi, A and Parhizkar, H., 2018. Performance analysis of microelectromechanical thrusters using a direct simulation Monte Carlo solver. *Proceedings of the Institution of Mechanical Engineers, Part G: Journal of Aerospace Engineering*, 232(7), p. 1212-1222. <https://doi.org/10.1177/0954410017691066>
- [4] Ma, K., Zhang, Z, Liu Y, and Jiang Z., 2020. Aerodynamic principles of shock-induced combustion ramjet engines. *Aerospace Science and Technology*, 103, p. 105901. <https://doi.org/10.1016/j.ast.2020.105901>
- [5] Wu, K., Zhang S., Luan, M., and Wang J., 2020. Effects of flow-field structures on the stability of rotating detonation ramjet engine. *Acta Astronautica*, 168, p. 174-181. <https://doi.org/10.1016/j.actaastro.2019.12.022>
- [6] Sun, L., Bian, F., Lei, X., Sh, D., Bao, F., 2023. Quantitative analysis of enhanced mixing and combustion by lobed mixer in a ramjet engine: Study using hyperbolic Lagrangian coherent structures. *Aerospace Science and Technology*, 140, p. 108471. <https://doi.org/10.1016/j.ast.2023.108471>
- [7] Choubey, G., Yuvarajan, D., Huang, W., Yan, L., Babazadeh, H., Pandey, K., 2020. Hydrogen fuel in scramjet engines-a brief review. *International Journal of Hydrogen Energy*, 45(33), p. 16799-16815.



- <https://doi.org/10.1016/j.ijhydene.2020.04.086>
- [8] Das, N., Pandey, K, and Sharma, K., 2021. A brief review on the recent advancement in the field of jet engine-scrumjet engine. *Materials Today: Proceedings*, 45, p. 6857-6863.  
<https://doi.org/10.1016/j.matpr.2020.12.1035>
- [9] Tylman, I., Grabowy, R. and Rećko, M., 2019. Thrust and ignition control of valveless pulse jet engine. 20th International Carpathian Control Conference (ICCC). IEEE.  
<https://doi.org/10.1109/CarpathianCC.2019.8766007>
- [10] Lisanti, J.C., Zhu, X. Guiberti, T.F. and Roberts, W. L., 2022. Active Valve Resonant Pulse Combustor for Pressure Gain Combustion Applications. *Journal of Propulsion and Power*, 38(2), p. 171-180.  
<https://doi.org/10.2514/1.B38226>
- [11] Modi, S., Khinchi, S., Rajpurohit, N. and Rami, A., 2021. Design and development of valveless pulsejet engine. In 2020 3rd International Conference on Energy, Power and Environment: Towards Clean Energy Technologies, (pp. 1-6). IEEE.  
<https://doi.org/10.1109/ICEPE50861.2021.9404374>
- [12] Rajashekar, C., Raghukumar, HS., Natarajan, R., Jeyaseelan, AR., Isaac, JJ., 2021. Development of a Retro-Reflective Screen-Based Large-Field High-Speed Shadowgraph Flow Visualization Technique and Its Application to a Hydrogen-Fueled Valveless Pulsejet Engine. In *Proceedings of the National Aerospace Propulsion Conference*. Springer. [https://doi.org/10.1007/978-981-15-5039-3\\_21](https://doi.org/10.1007/978-981-15-5039-3_21)
- [13] Ghulam, M.M., Muralidharan, S., Anand, V., Prisell, E., Gutmark, E., 2024. Operational mechanism of valved-pulsejet engines. *Aerospace Science and Technology*, 148, p. 109060.  
<https://doi.org/10.1016/j.ast.2024.109060>
- [14] Anand, V., Jodele, J., Prisell, E., Lyrsell, O., Gutmark, E., 2020. Dynamic features of internal and external flowfields of pulsejet engines. *AIAA Journal*, 58(10), p. 4204-4211.  
<https://doi.org/10.2514/1.J059685>
- [15] Anand, V., Jodele, J., Prisell, E., Lyrsell, O., and Gutmark, E., 2021. Visualization of Valved Pulsejet Combustors and Evidence of Compression Ignition. *Flow, Turbulence and Combustion*, 106(3), p. 901-924.  
<https://doi.org/10.1007/s10494-020-00203-4>
- [16] Matsuoka, K., Yageta, J., Nakamichi, T., Kasahara, J., Yajima, T., and Kojima, T., 2011. Inflow-driven valve system for pulse detonation engines. *Journal of propulsion and power*, 27(3), p. 597-607.  
<https://doi.org/10.2514/1.47421>
- [17] Nguyen, V., Teo, CJ., Chang, PH., Li, JM., and Khoo, BC., 2019. Numerical investigation of the liquid-fueled pulse detonation engine for different operating conditions. *Shock Waves*, 29, p. 1205-1225.  
<https://doi.org/10.1007/s00193-019-00898-z>
- [18] Alam, N., Sharma, K. and Pandey, K., 2019. Numerical investigation of flame propagation and performance of obstructed pulse detonation engine with variation of hydrogen and air. *Journal of the Brazilian Society of Mechanical Sciences and Engineering*, 41(11), p. 502.  
<https://doi.org/10.1007/s40430-019-2024-0>
- [19] Suchocki, J., Yu, S., Hoke, J., Naples, A., Schauer, F., Russo, R., 2012. Rotating detonation engine operation. In 50th AIAA aerospace sciences meeting including the new horizons forum and aerospace exposition.  
<https://doi.org/10.2514/6.2012-119>
- [20] Wakita, M., Tamura, M., Sajiki, K., Totani, T., Nagata, H., 2013. Detonation Transition Around Cylindrical Reflector of Pulse Detonation Engine Initiator. *Journal of Propulsion and Power*, 29(4), p. 825-831.  
<https://doi.org/10.2514/1.B34704>
- [21] Trzeciak, A. and Gieras, M., 2020. Temperature estimating method for exhaust gases in valveless pulsejet engine. *Combustion Engines*, 59(3).  
<http://dx.doi.org/10.19206/CE-2020-301>
- [22] Agarwal, A. and Pitso, I., 2020. Modelling & numerical exploration of pulsejet engine using eddy dissipation combustion model. *Materials today: proceedings*, 27, p. 1341-1349.  
<https://doi.org/10.1016/j.matpr.2020.02.620>
- [23] Anand, V., Jodele, J., Knight, E., Prisell, E., Lyrsell, O., Gutmark, E., 2018. Dependence of pressure, combustion and frequency characteristics on valved pulsejet combustor geometries. *Flow, Turbulence and Combustion*, 100, p. 829-848.  
<https://doi.org/10.1007/s10494-017-9875-1>
- [24] Yungster, S., Paxson, D.E. and Perkins, H. D., 2018. Computational study of compact ejector-enhanced resonant pulse combustors. *Propulsion Conference*.  
<https://doi.org/10.2514/6.2018-4786>
- [25] Qatomah, M., Lisanti, J.C. and Roberts, W., 2018. Influence of fuel composition on the operation of a liquid fueled resonant pulse



- combustor. Propulsion Conference. <https://doi.org/10.2514/6.2018-4571>
- [26] Min, L., Ling, Y. and Wen-xiang, C., 2016. Experiment analysis of combustion performance in pulse jet engine. Energy procedia, 100, p. 248-252. <https://doi.org/10.1016/j.egypro.2016.10.173>
- [27] Suganya, R., 2015. Design and analysis of improved pulse jet engine. Journal of Scientific Engineering and Technologi Research, 4(14), p. 2684.
- [28] Nazarpour A. and Fathali M, 2015. Investigation of the Impact of Geometric Characteristics of a Valveless Pulse Jet Engine on Thrust. Aerospace Science and Technology Journal [in persian].
- [29] Taherishad M., Bazazadeh M., Adami M., Hamledari J., 2014. Design, Construction, and Testing of a Valveless Pulse Jet Engine, Investigation of Geometric Parameters on Output Thrust, and Combustion Study. International Conference on Iranian Aerospace [in persian]
- [30] Rajashekar, C., Raghukumar, HS., Reddy, M., Bhaskaran, M., and Isaac, J.J., 2013. High-Speed Shadowgraph Visualisation of Flow in a Miniature Hydrogen-Fuelled Valveless Pulsejet Engine. In Proceedings of International Conference on Intelligent Unmanned Systems.
- [31] Evans, R. and Alshami, A., 2009. Pulse jet orchard heater system development: Part I. Design, construction, and optimization. Transactions of the ASABE, 52(2), p. 331-343.
- [32] Paxson, D. and Dougherty K., 2008. Operability of an ejector enhanced pulse combustor in a gas turbine environment. In 46th AIAA Aerospace Sciences Meeting and Exhibit. <https://doi.org/10.2514/6.2008-119>
- [33] Geng, T., Kiker Jr A., Ordon, R., Kuznetsov, AV., Zeng, TF., Roberts, WL., 2007. Combined numerical and experimental investigation of a hobby-scale pulsejet. Journal of propulsion and power. 23(1), p. 186-193. <https://doi.org/10.2514/1.18593>
- [34] Nakano, T., Matsuo, S., Teramoto, K. and Setoguchi, T., 2006. Effect of exit geometry of tail pipe on the performance of pulse jet engines. Journal of Thermal Science, 15, p. 263-268. <https://doi.org/10.1007/s11630-006-0263-8>
- [35] Litke, P., Schauer, F., Paxson, D., Bradley, R., Hoke, J., 2005. Assessment of the Performance of a Pulsejet and Comparison with a Pulsed-Detonation Engine. in 43rd AIAA Aerospace Sciences Meeting and Exhibit. <https://doi.org/10.2514/6.2005-228>
- [36] Blomquist, C., 1982. Experimental gas-fired pulse-combustion studies.
- [37] Mason, S., Miller, R. and Taylor, M., 2008. Fluid Mechanics of Pulse Pressure-Gain Combustors. In 46th AIAA Aerospace Sciences Meeting and Exhibit. <https://doi.org/10.2514/6.2008-118>
- [38] John, J.E.A. and Keith, T.G., 2006. Gas Dynamics. Pearson Prentice Hall.
- [39] Uskov, V.N. and Mostovkykh, P.S., 2010. Interference of stationary and non-stationary shock waves. Shock Waves, 20(2), p. 119-129. <https://doi.org/10.1007/s00193-009-0243-5>
- [40] Bulat, P.V. and Uskov, V.N., 2016. Gas-dynamic waves and discontinuities. International Electronic Journal of Mathematics Education, 11(5), p. 1101-1111.
- [41] Atmosphere, U.S., 1976. National Oceanic and Atmospheric Administration (NOAA). National Aeronautics and Space Administration (NASA). United States Air Force, Washington, DC.
- [42] Hosseini, S., Vaziry-Zanjany, M.A., Ovesy, H.R., and Lekzian, E., 2023. Multi-Objective Multidisciplinary Design Optimization of Regional Truss-Braced Wing Jet Aircraft. In Proceedings of the Aerospace Europe Conference. <http://dx.doi.org/10.13009/EUCASS2023-007>
- [43] Lekzian, E., Farshi, H. and Modanlou, R., 2023. Aerothermodynamic off-design performance study of a fixed double bypass duct turbofan engine. The Journal of Engine Research, 70(3), p. 62-75. <https://doi.org/10.22034/er.2024.201925.4.1022>
- [44] Lekzian, E. and Modanlou, R., 2024. Performance Study of Separate Exhaust Innovative Turbofan Engine Configurations with the Control Mechanism of a Baseline Engine. AUT Journal of Mechanical Engineering, 8(3), pp. 257-272. <https://doi.org/10.22060/ajme.2024.2315.4.6107>
- [45] Hosseini, S., Zanjany, M.A.V., Oveysy, H.R. and Lekzian, E., 2024. Application of Lambda Framework for Aircraft Multidisciplinary Design, Analysis and Optimization. In 34th Congress of the International Council of the Aeronautical Sciences, ICAS 2024, Florence, Italy.